Defect and Diffusion Forum
ISSN: 1662-9507, Vol. 434, pp 143-147
doi:10.4028/p-tZsV2d

Submitted: 2023-10-02
Revised: 2024-04-14
Accepted: 2024-04-15
Online: 2024-08-22

Development of 3-Channel Inspection Analysis Technique for Defects of SiC Epitaxial Wafers Using Optical Inspection, Photoluminescence and X-Ray Topography

Junji Senzaki[a*], Junichi Nishino[b] and Tsutomu Osanai[c]

Advanced Power Electronics Research Center, National Institute of Science and Technology, 16-1 Onogawa, Tsukuba, Ibaraki, Japan

[a]junji-senzaki@aist.go.jp, [b]nishino.junichi@aist.go.jp, [c]t-osanai@aist.go.jp

Keywords: defect, inspection technique, optical inspection, photoluminescence, X-ray topography

Abstract. 3-channel analysis technique consisting of optical inspection, photoluminescence and X-ray topography methods for defect inspection of SiC epitaxial wafers has been investigated. The effectiveness of SiC wafer inspection image correction to enable automatic defect analysis is verified. Next, it is shown that the 3-channel analysis technique improves SiC defect inspection accuracy compared to conventional 2-channel analysis one.

Introduction

One of the essential efforts to realize the social implementation of SiC power devices is the development of practical measurement technology that can inspect the quality of SiC wafers with "high precision," "high-speed," and "non-destructive." In general, Optical inspection (OI) method and photoluminescence (PL) method are widely used for defect inspection of SiC epitaxial wafers, but its inspection accuracy is degraded due to non-detection and/or erroneous detection for some defect classes. As an effective solution to this problem, we propose a 3-channel inspection analysis technique for SiC epitaxial layer defects, which consists of the OI method, PL method, and X-ray topography (XRT) method. The concept of the technique and manual analysis result have been reported [1,2], but an automated analysis that integrated the three types of inspection data was not possible due to deviations in the detection position of defects in XRT observation images caused by warpages of SiC epitaxial wafer and crystal lattice plane. In this study, we report the defect detection position correction method in the XRT observation image, and the verification result of SiC epitaxial defect inspection accuracy by the 3-channel automated analysis.

Experimental

The developed analysis technique integrates each inspection data obtained using SICA88 (Lasertec) for OI observation and PL observation, and XRTmicron (Rigaku) for XRT observation, and automatically classifies defects of SiC epitaxial layer. Five commercially available n-type 4H-SiC epitaxial wafers with an epitaxial layer thickness of 10 μm and a diameter of 6 inches were used as test samples. We performed the PL observation in the near-infrared wavelength region and the XRT observation under the diffraction condition of $\boldsymbol{g} = 0008$. To verify the defect detection accuracy, the Advanced SICA Viewer was used, which can import and comprehensively evaluate observation images acquired by various wafer inspection apparatuses. The XRT image correction for 3-channel analysis was carried out as follows. The coordinates of five or more SiC epitaxial defects were selected as alignment points from the entire wafer image obtained by each of the XRT method, OI method and PL method, and then a corrected XRT image was created by image processing based on the coordinate information.

Results and Discussion

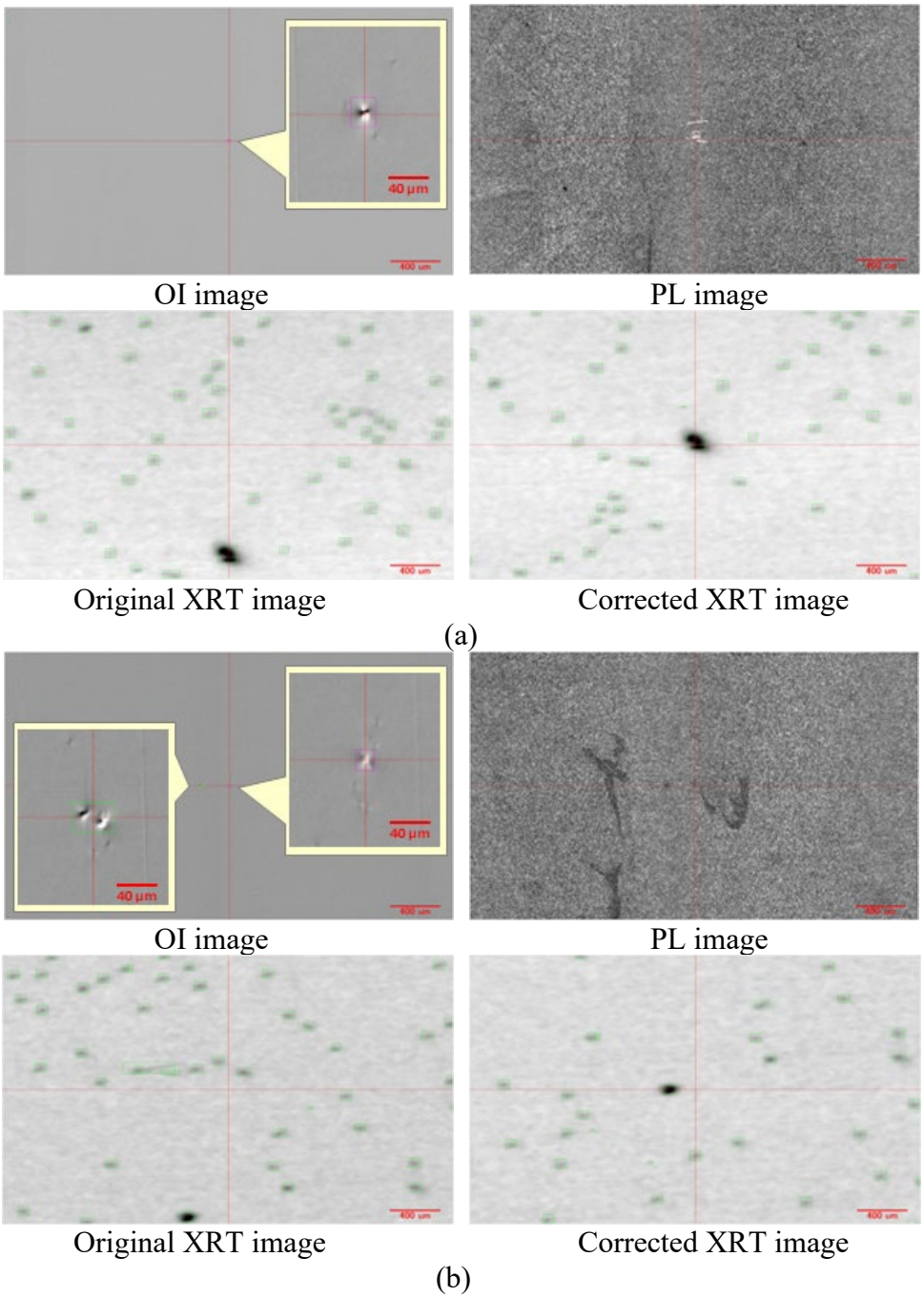

Fig. 1. Observation images of defect inspected as micropipe acquired on the same wafer by wafer inspection equipment. In (a), a micropipe was inspected correctly, while in (b), a particle inclusion was incorrectly inspected.

Figure 1 shows observation images of defect inspected as a micropipe on the same wafer using a 2-channel inspection analysis technique consist of OI and PL observations. In both cases, the OI image on the top left and the PL image on the top right were acquired by SICA88, and the XRT image on the bottom left was acquired by XRTmicron. Another XRT image on the bottom right was created by correcting the original XRT image on the bottom left with respect to the X-Y coordinates of the OI image on the top left. In the 2-channel analysis, one and two large pits detected in the OI images in (a) and (b) were inspected as micropipes, respectively. In the 3-channel analysis that added the XRT images to this 2-channel analysis result, it was confirmed that each large pit detected in (a) and on the left side in (b) was a micropipe because a large dark contrast was observed at the same position in the corrected XRT image. On the other hand, no contrast is observed in the corrected XRT image at the same position as the large pit detected on the right side in (b), indicating that the detected defect

was not a micropipe but a particle inclusion, so-called downfall. Besides, differences in the coordinates of the micropipe detected in the OI image and the original XRT image are 920 μm in the downward direction in (a) and 1057 μm in the lower left direction in (b), respectively. This indicates that the detection position difference and direction differ depending on the defect even on the same wafer in the original XRT image. On the other hand, there is almost no difference in the defect detection position in the corrected XRT image, resulting in the successful XRT image correction. The verification result of the defect detection coordinate difference within the wafer plane for all wafers is shown in Fig. 2.

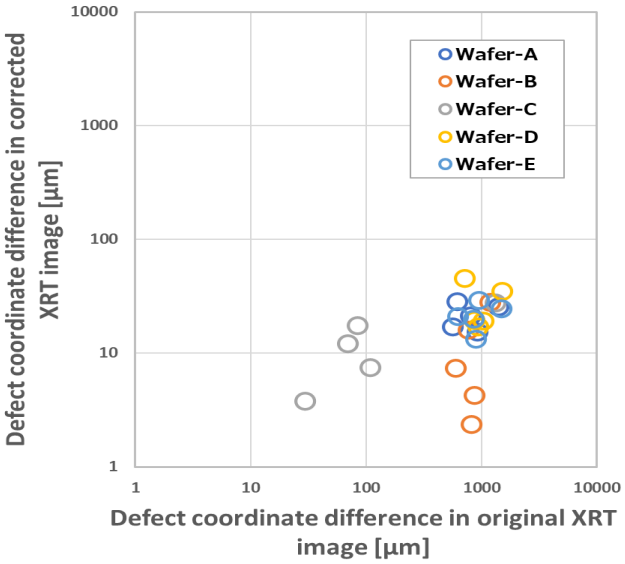

Fig. 2. Comparison of defect detection coordinate difference with and without XRT image correction on OI images. The defect detection coordinate difference was verified at 5 points on each wafer.

The horizontal and vertical axes of the figure show the coordinate differences of the same defect in the original and corrected XRT images, respectively, with respect to the defect in the OI image. Wafer in-plane variations in defect detection coordinate differences were examined at the center of each test wafer, and at five points, left, right, top and bottom, which are approximately the same distance from the center. As a result, in the original XRT image, 4 out of 5 wafers had a very large defect detection coordinate difference of around 1000 μm, while in the corrected XRT image, all wafers achieved a coordinate difference of 50 μm or less. This verification result indicates that 3-channel automated analysis for defects based on defect detection coordinates is possible by using the corrected XRT images.

Next, the effect of 3-channel automated analysis on micropipe detection accuracy is verified. A micropipe was selected as a test target, and the verification work was carried out according to the following judgement rules. For each micropipe inspected by the 2-channel analysis with the OI and PL results, when a large dark contrast was observed in the corrected XRT image within the defect detection coordinate matching range set as the judgment condition, it was judged as a micropipe. On the other hand, when a large contrast was not observed, it was determined that the detected defect was not a micropipe. Figure 3 shows the dependence of defect detection coordinate matching range on micropipe inspection accuracy for five SiC epitaxial wafers. In the figure, the horizontal axis indicates the defect recognition accuracy, and the vertical axis indicates the defect detection accuracy. Note that the closer the analysis result is plotted to the upper right corner of the graph, the higher the defect inspection accuracy is. For all wafers, the filled circles show the 2-channel analysis results by OI and PL methods. Open symbols represented by ○, □, △, ◇, and ∗ show the results of 3-channel analysis under the conditions that the defect detection coordinate matching range is 100 μm, 70 μm, 50 μm, 30 μm, and 10 μm, respectively. For all wafers, the 3-channel analysis improves the accuracy of defect detection, but the smaller the matching range, the lower the defect recognition accuracy, confirming that there is an optimum condition for maximum inspection accuracy of micropipe. In

addition, this trend differs depending on the wafer quality. Wafer-A and -B, which have low epitaxial defect density, achieved micropipe inspection accuracy of 100% under the matching range condition of 100 μm. However, Wafer-C, -D, and -E with high epitaxial defect density did not achieve a remarkable improvement in inspection accuracy even if the matching range conditions were changed. This is because as the number of detected defects increases, the number of erroneous judgments in the 3-channel analysis also increases.

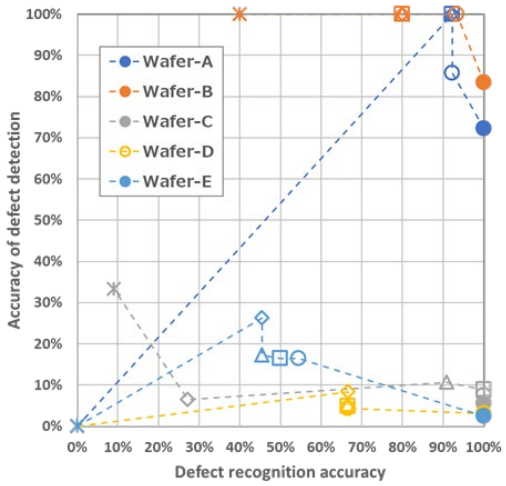

Fig. 3. Effect of defect detection coordinate matching range on micropipe inspection accuracy. Filled circles indicate 2-channel analysis results using OI and PL images. Open symbols indicate the results of 3-channel analysis, and ○, □, △, ◇, and ∗ indicate that the defect detection coordinate position difference is within 100 μm, within 70 μm, within 50 μm, within 30 μm, and within 10 μm, respectively.

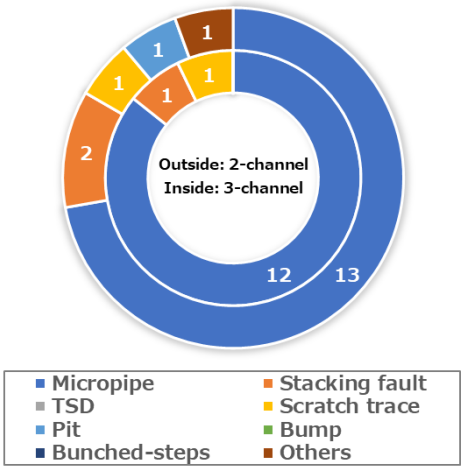

Fig. 4. Doughnut charts of defect inspection results for micropipes in Wafer-A. The outer and inner charts are 2-channel and 3-channel analysis results, respectively. The defect detection coordinate matching range in 3-channel analysis is 100 μm.

Figure 4 shows the verification results of the micropipe inspection in Wafer-A when the defect detection coordinate matching range is 100 μm. In the figure, it is indicated that the 2-channel inspection using the OI image and PL image detected 18 micropipes as shown in the outer doughnut chart, while the 3-channel inspection detected 14 micropipes in the inner chart. Visual inspection of all the detected micropipes revealed that 5 out of 18 micropipes were erroneously detected in the 2-channel inspection, and two stacking faults, one scratch trace, one pit, and the other were detected as micropipes. On the other hand, in the 3-channel inspection, 2 out of 14 micropipes were falsely detected, and the defects misidentified as micropipes were one stacking fault and one scratch trace. This result indicates that the accuracy of micropipe detection improved from 72% for the 2-channel inspection to 86% for the 3-channel one. However, one micropipe was detected to be in another defect class in the corrected XRT image, so it was not judged as a micropipe in the 3-channel inspection, and as a result, the recognition accuracy decreased to 92%.

Summary

This research reported verification results of a 3-channel analysis for micropipe in SiC epitaxial wafers using OI, PL and XRT methods. Regarding the detection coordinate difference of SiC epitaxial defects in the corrected XRT image, we confirmed that a “coordinate difference of 100 μm or less” was achieved. A comparison of inspection accuracy for SiC epitaxial defects (2-channel analysis vs. 3-channel analysis) confirmed that the 3-channel analysis improved the SiC epitaxial defect detection accuracy. These results suggest the realization of highly accurate wafer quality inspection by comprehensively analyzing multiple inspection data, and it is expected that practical wafer quality technology will be established by improving the analysis accuracy of each data.

Acknowledgement

This work has been partially implemented under a joint research project of Tsukuba Power Electrics Constellations (TPEC).

References

[1] I. Kamata, X. Zhang, H. Tsuchida, Photoluminescence of Frank-type defects on the basal plane in 4H-SiC epilayers, Appl.Phys. Lett. 97 (2010) 172107.

[2] T. Yamashita, H. Matsuhata, Y. Miyasaka, M. Odawara, K. Momose, T. Sato, M. Kitabatake, Characterization of (4,4)- and (5,3)-type stacking faults in 4deg.-off 4H-SiC epitaxial wafers by synchrotron X-ray topography and by photo-luminescence spectroscopy, Mater. Sci. Forum, 740-742 (2013) 585-588.

[3] M. Nagano, I. Kamata, H. Tsuchida, Photoluminescence imaging and discrimination of threadingdislocations in 4H-SiC epilayers, Mater. Sci. Forum, 778-780 (2014) 313-318.

[4] IEC standard, Non-destructive recognition criteria of defects in silicon carbide homoepitaxial wafer for power devices - Part 1: Classification of defects, IEC 63068-1:2019 (2019).

[5] IEC standard, Non-destructive recognition criteria of defects in silicon carbide homoepitaxial wafer for power devices - Part 2: Test method for defects using optical inspection, IEC 63068-2:2019 (2019).

[6] J. Senzaki, A. Maeda, S. Fujiki, H. Seki, K. Morikawa, Y. Ueji, K. Omote, Development in advanced inspection system for detecting defects in SiC epitaxial wafers: presented at the 18th Conference on Defects - Recognition, Imaging and Physics in Semiconductors, Belrin, Germany, 2019 (unpublished).

[7] J. Senzaki, R. Kosugi, K. Masumoto, T. Mitani, T. Kuroiwa, H. Yamaguchi, Influence of SiC epitaxial wafer quality on yield of 1.2kV SiC-DMOSFETs, in Proceedings of the 2022 IEEE International Reliability Physics Symposium (IRPS), edited by IEEE, (2022) P63.

[8] JEITA standard, Non-destructive recognition procedures of defects in Silicon Carbide Wafer - Part 3: The measurement method for defects in Silicon Carbide Wafer using photoluminescence, JEITA EDR-4712/300 (2018).

[9] JEITA standard, Non-destructive recognition procedures of defects in Silicon Carbide Wafer - Part 4: The guideline for identifying and evaluating defects in Silicon Carbide Wafer using a combined method of optical inspection and photoluminescence, JEITA EDR-4712/400 (2020).

[10] JEITA standard, Non-destructive recognition procedures of defects in Silicon Carbide Wafer - Part 5: The measurement method for defects in Silicon Carbide Wafer using X-ray topography, JEITA EDR-4712/500 (2023).